



**HAL**  
open science

## **Radiation-induced oxidative damage to the DNA-binding domain of the lactose repressor**

Nathalie Gillard, Stephane Goffinont, Corinne Buré, Marie Davidkova,  
Jean-Claude Maurizot, Martine Cadene, Melanie Spotheim-Maurizot

► **To cite this version:**

Nathalie Gillard, Stephane Goffinont, Corinne Buré, Marie Davidkova, Jean-Claude Maurizot, et al..  
Radiation-induced oxidative damage to the DNA-binding domain of the lactose repressor. *Biochemical  
Journal*, 2007, 403 (3), pp.463-472. 10.1042/BJ20061466 . hal-00478672

**HAL Id: hal-00478672**

**<https://hal.science/hal-00478672>**

Submitted on 30 Apr 2010

**HAL** is a multi-disciplinary open access archive for the deposit and dissemination of scientific research documents, whether they are published or not. The documents may come from teaching and research institutions in France or abroad, or from public or private research centers.

L'archive ouverte pluridisciplinaire **HAL**, est destinée au dépôt et à la diffusion de documents scientifiques de niveau recherche, publiés ou non, émanant des établissements d'enseignement et de recherche français ou étrangers, des laboratoires publics ou privés.

## **Radiation-induced oxidative damage to the DNA-binding domain of the lactose repressor**

Nathalie Gillard <sup>a</sup>, Stephane Goffinont <sup>a</sup>, Corinne Buré <sup>a</sup>, Marie Davidkova <sup>b</sup>,  
Jean-Claude Maurizot <sup>a</sup>, Martine Cadene <sup>a</sup>, and Melanie Spothem-Maurizot <sup>a,1</sup>

*<sup>a</sup>Centre de Biophysique Moléculaire, CNRS, rue C. Sadron, 45071 Orléans  
Cedex 2, France, and Nuclear Physics Institute, Department of Radiation  
Dosimetry, Na Truhlarce 39/64, CZ-18086, Praha 8, Czech Republic*

Paper No BJ2006/1466

### **Corresponding author**

Melanie Spothem-Maurizot

Centre de Biophysique Moléculaire, CNRS, rue C. Sadron,  
45071 Orléans Cedex 2,

Phone : (33) 2 38 25 55 75

Fax : (33) 2 38 63 15 17

email : spotheim@cnrs-orleans.fr

### **Short title**

Radiation damage to lactose repressor headpiece

### **Keywords**

Ionising radiation, protein oxidation, mass spectrometry, Monte Carlo simulation, radiolytic  
attack

Gillard, N., Goffinont, S., Buré, C., Davidkova, M., C. Maurizot, J-C., Cadene, M. and Spothem-Maurizot, M. Radiation-induced damage to the DNA-binding domain of the lactose repressor.

## Abstract

Understanding the cellular effects of radiation-induced oxidation requires the unravelling of key molecular events, particularly damage to proteins with important cellular functions. *Escherichia coli* lactose operon is a classical model of gene regulation systems. Its function mechanism involves the specific binding of a protein, the repressor, to a specific DNA sequence, the operator. We have shown previously that upon irradiation with  $\gamma$  rays in solution, the repressor loses its ability to bind the operator. Water radiolysis generates hydroxyl radicals (OH radicals) which attack the protein. Damage of the repressor DNA binding domain, called the headpiece, is most probably responsible of this loss of function. Using circular dichroism (CD), fluorescence spectroscopy and a combination of proteolytic cleavage with mass spectrometry, we examine the state of the irradiated headpiece. CD measurements reveal a dose-dependent conformational change involving metastable intermediate states. Fluorescence measurements show a gradual degradation of tyrosines. Mass spectrometry was used to count the number of oxidations in different regions of the headpiece and to narrow down the parts of the sequence bearing oxidised residues. By calculating the relative probabilities of reaction of each amino acid with OH radicals, we can predict the most probable oxidation targets. By confronting the experimental results with the predictions we conclude that Tyr7, Tyr12, Tyr17, Met42 and Tyr47 are the most likely hot spots of oxidation. The loss of repressor function is thus correlated with chemical modifications and conformational changes of the headpiece.

## Introduction

Exposure to ionising radiation induces alterations in redox-sensitive metabolic processes, apoptosis, mutagenesis and carcinogenesis through very complex phenomena involving damage and repair of DNA as well as damage to other cellular components. Damage to DNA is considered as the critical event in the destructive effect of ionising radiation and therefore the type of DNA lesions, their distribution and their repair is largely studied [1]. However, DNA accomplishes its biological function by interacting with other cellular components, mainly proteins involved in replication, transcription, the regulation of gene expression, chromatin remodelling and epigenetic control. The physical integrity of DNA is maintained by interaction with structural proteins as well as repair proteins capable of reversing stress or metabolism-driven oxidative DNA lesions. DNA-binding proteins protect DNA from attack by the products of water radiolysis, particularly from the most aggressive one, the oxidising hydroxyl radical (OH<sup>•</sup> or OH radical). However, by interacting with the radicals, the proteins themselves get damaged to the point of losing function when exposed to doses of radiation higher than a system-dependent threshold. Protein damage has the potential to disrupt the function of DNA-protein complexes, leading to dramatic cellular effects. Moreover, the cell is endowed with DNA repair mechanisms, whereas there are far fewer opportunities for remediation for damaged proteins.

Radiation-induced damage to proteins has been the object of far fewer studies than DNA damage until now. Moreover, the OH radical is also one of the main ROS (reactive oxygen species) produced in cells upon oxidative stress. Protein oxidation induced by oxidative stress is known to be involved in aging, neurodegenerative processes and cardiovascular diseases [2]. Resistance to oxidation is a sought-after property for therapeutic proteins [3]. The similarities between protein oxidation induced by radiation and by oxidative stress broadens the scope of protein damage studies, especially in light of the discovery of a growing number of epigenetic effects.

Protein exposure to ionising radiations induces modifications of the side-chains of amino acids and peptide chain breaks. Many of these lesions and their mechanisms of formation have been identified [4, 5]. The amino acids with the highest reactivity toward OH radicals are cysteine, tryptophan, tyrosine, methionine and phenylalanine [6-8]. In a protein, the reactivity of amino acids is modulated by the accessibility of the residues to the OH radical. We have built a model of simulation of the radiolytic attack (RADACK) which takes into

account both the chemical reactivity of each amino acid toward the diffusing OH radicals and the accessibility of the reactive sites [9-11]. RADACK can be used to calculate the probability of reaction of each residue with OH radical for proteins with known three-dimensional structure as determined by NMR or crystallography.

We have previously reported the radiation-induced dysfunction of several DNA-protein complexes: the *Escherichia coli* (*E. coli*) lactose operator-repressor complex, the complex between MC1, a DNA structuring protein of the archaeobacterium *Methanosarcina thermophila* and its specific DNA sequence, as well as the complex between a DNA bearing an analogue of an abasic site and the repair protein Fpg of *Lactococcus lactis*. When irradiated with  $\gamma$  rays, the three studied complexes are disrupted mainly due to protein damage. The irradiation of the free proteins induces the loss of their ability to bind DNA at even lower doses than those necessary to the disruption of the irradiated complexes due to the protection of the proteins by the bound DNA [10, 12-14].

After investigating the damage to DNA upon the irradiation of the *E. coli* lactose operator-repressor complex [15, 16], we focus here on the damage of the protein.

The *E. coli* lactose repressor is a homotetrameric protein (monomer of 360 amino acids) organised in two dimers. It contains the following domains : the tetrameric core (formed by the C-terminal regions of the four monomers and containing amino acids 59-360) and four headpieces (each one being the N-terminal region of the monomer and containing amino acids 1-49) linked to the core by a hinge which is unfolded in the free state (amino acids 50-58). The headpiece contains three  $\alpha$  helices (residues Leu6-Ala13, Tyr17-Val24, and Ala32-Leu45) linked by loops. The first two helices form, together with their connecting loop, the helix-turn-helix (HTH) motif which directly interacts with the major groove of operator DNA. The second helix is called the recognition helix [17-19]. Both headpiece domains of a dimer can bind one operator DNA, and in this case the hinge becomes structured [20-22]. It should be noted that the headpiece does not contain any cysteine, tryptophan, or phenylalanine residues.

Using a phenomenological model accounting for our experimental results, we have previously shown that a repressor ceases to bind DNA when both its dimers are inactivated by irradiation. Further, each dimer is inactivated when at least one monomer is inactivated. Finally, one monomer is inactivated with as little as two radiation-induced damages. We have also concluded that the two critical damages may result from the oxidation of amino acids side chains, probably located in the headpieces, by OH radicals [13].

In the present study we investigate in detail the state of an irradiated headpiece. The overall conformation and the modifications of amino acid side-chains are examined using a combination of circular dichroism, fluorescence spectroscopy, and mass spectrometry. The damages observed experimentally are discussed in relation with the predictions of the RADACK model.

## Materials and Methods

### *Headpiece preparation*

The DNA sequence coding for the headpiece was inserted in the pET24a(+) plasmid (Novagen) and the peptide was expressed in the BL21(DE3) overproducing strain of *E. coli* (Stratagene). After expression, cells were lysed by sonication in a lysis buffer (50 mM potassium phosphate buffer pH 7.5, 250 mM NaCl, 1mM EDTA, 1 mM PMSF, 5 mM mercapto-ethanol, 5% glycerol) in a ratio of 6g cell/60 ml buffer. After centrifugation (30 minutes, 12000 rpm), the supernatant was treated with ammonium sulfate and centrifuged in the same conditions. The resulting pellet was dissolved in 1 liter SP0 buffer (50 mM phosphate buffer pH 7.5, 1 mM PMSF, 5 mM mercapto-ethanol, 5% glycerol). The extract was then loaded onto a cation-exchanging sulfopropyl column (HiLoad<sup>TM</sup> 16/10 SP Sepharose<sup>TM</sup> HP, Amersham Biosciences) equilibrated in SP1 buffer (50 mM phosphate buffer pH 7.5, 100 mM NaCl, 1 mM PMSF, 5 mM mercapto-ethanol, 5% glycerol). After washing with SP1 buffer, the protein was eluted with a SP1/SP2 gradient (SP2 buffer: 50 mM tampon phosphate pH 7.5, 600 mM NaCl, 1 mM PMSF, 5 mM mercapto-ethanol , 5% glycerol). The fractions containing the headpiece were then precipitated in 75% ammonium sulfate. The protein pellet was dissolved in 4 ml AcA buffer (25 mM Hepes pH7.5, 1 M NaCl, 5 mM mercapto-ethanol, 0.1 mM PMSF, 5% glycerol) and loaded on a gel filtration column (Ultrogel® AcA 54). After elution with AcA buffer, the fractions containing the protein were precipitated by ammonium sulfate. The headpiece was finally stored at -20°C in a 1 M Tris-HCl, pH 7.45, 10 mM 1,4-dithiothreitol, and 20 % glycerol buffer. Before use, headpiece aliquots were buffer-exchanged by elution on a Sephadex G-25 column. The final headpiece concentration was determined by spectrophotometric measurements, assuming that  $\epsilon_{280} = 4800 \text{ M}^{-1} \text{ cm}^{-1}$ .

### ***Headpiece irradiation***

Samples of headpiece solutions were contained in polypropylene micro tubes (Eppendorf 1.5 ml). The irradiated volumes were typically 10-100  $\mu$ l. The tubes were immersed in an ice bath and irradiated in a  $^{137}\text{Cs}$  irradiator (IBL437, CisBio International) delivering 0.6 MeV  $\gamma$  rays at a dose rate of 9 Gy  $\text{min}^{-1}$ . For CD and fluorescence measurements the samples were irradiated directly in the spectrometer quartz cells. Dosimetry was performed using the Fricke's chemical dosimeter.

### ***Circular dichroism***

The headpiece conformation was studied by circular dichroism with a JASCO's J-810 dichrograph. The spectra, in the wavelength range 200-250 nm, were recorded in quartz cells of 2 mm path length. Irradiation and CD measurements were realised with samples concentration of 29  $\mu$ M in a 25 mM ammonium cacodylate buffer (pH 7.25).

### ***Fluorescence measurements***

Fluorescence emission spectroscopy was used to study damage to tyrosine residues and search for dityrosine formation. Emission spectra (excitation wavelength 275 nm for tyrosine study, 320 nm for dityrosine, 5 nm bandwidth) were recorded in silica cells of 5 mm path length using a Jobin-Yvon Fluoromax 2 spectrofluorimeter (from 280 to 320 nm for tyrosine formation and from 360 to 490 nm for dityrosine formation). Irradiation and fluorescence measurements were realised at a headpiece concentration of 29  $\mu$ M in a 25 mM ammonium cacodylate buffer (pH 7.25).

### ***Theoretical calculations: RADACK model***

The stochastic simulation model RADACK (9-11) was applied for the determination of the probability of each residue to react with hydroxyl radicals. The calculation is based on the structure of the headpiece determined by NMR, available in the PDB Databank with the code 1LQC (18). Smoluchovski's spheres with radius proportional to the reactivities of the amino acids were placed on the reactive hydrogen atoms of all amino acids. All non-reactive atoms are represented by Van der Waals spheres. The relative probability of reaction between freely diffusing OH radicals and the amino acids of the headpiece was determined.

### ***Proteolytic cleavage***

The side chain modifications were studied by a combination of proteolytic cleavage and mass spectrometry. Samples of headpiece protein at a final concentration of 20  $\mu$ M were digested with endoproteinase GluC (Roche) in a 25 mM ammonium cacodylate buffer, 10

mM CaCl<sub>2</sub>, 5 mM DTT, 0.5 mM EDTA, 50 mM NaCl (pH7.6) for 150 minutes, at 37°C using an enzyme-headpiece ratio of [1:25] (w/w), and alternatively with endoproteinase ArgC (Roche) in the same buffer at 25°C and in an enzyme-headpiece ratio of [1:10] (w/w).

### ***Mass spectrometry***

#### ***a) MALDI-TOF analysis***

The native and irradiated headpieces were analysed by matrix assisted laser desorption ionisation – time of flight mass spectrometry (MALDI-TOF MS) without further purification. The whole protein was first analysed to follow global patterns of irradiation damage. The headpiece was further characterised after proteolysis to identify peptides bearing radiation-induced oxidations.

The sample stage was coated using the ultra-thin layer method [23]. A matrix solution of water-acetonitrile [2:1] (v/v) saturated with  $\alpha$ -cyano-4-hydroxy-cinnamic acid, and containing an internal standard mixture of bradykinin, neurotensin and insulin (average masses of 904.5 Da, 1672.9 Da and 3494.6 Da, respectively) was freshly prepared. Samples were diluted 20-fold with this matrix solution and a 0.5  $\mu$ l aliquot spotted onto the sample stage. As soon as matrix-analyte co-crystals formed to homogeneity, the excess solution was removed by vacuum aspiration. MALDI-TOF analysis (Autoflex, Bruker) was performed in linear mode with delayed extraction. The data were acquired from accumulation of 200 laser shots (N<sub>2</sub> laser, 337 nm) with external calibration in Flex Control software. Spectra were calibrated internally and further processed using Flex Analysis software (Bruker).

#### ***b) ESI-IT analysis***

Samples of proteolysed headpiece were desalted on C<sub>18</sub> ZIP-TIP™ (Millipore). The resin was washed with a 50% water, 50% acetonitrile solution and equilibrated with 0.1% aqueous trifluoroacetic acid (TFA). The samples were acidified with 2% formic acid and loaded onto the resin. The resin was washed with a 5% methanol, 95% water, 0.1% TFA solution and the peptides eluted with a 30% water, 70% acetonitrile, 0.1% formic acid solution. Desalted samples were further diluted 5-fold with the same solution and analysed by electrospray ionisation – ion trap mass spectrometry (ESI-IT MS) (Esquire HCT, Bruker). The peptide mixture was analysed in MS mode with external calibration and appropriate peptide ions were selected for fragmentation with acquisition times of 6 minutes and a 2.5 Da isolation window. MS/MS spectra were further processed using Data Analysis software from Bruker.



## Results

### *Circular dichroism study of the headpiece conformation*

The headpiece was irradiated in the dose range 0-2000 Gy. For each dose, the CD spectrum was recorded from 200 to 250 nm at 4°C. As shown in Figure 1, the CD intensity decreases upon irradiation and the maximum negative intensity is displaced toward shorter wavelengths. An isodichroic point is observed at 204 nm. The inset shows the normalised variation of ellipticity at 220 nm.

Furthermore, the thermal stability of the peptide was assayed by performing denaturation - renaturation cycles. Non-irradiated or irradiated headpiece samples were thermally denatured and renatured in the cell of the dichrograph : from 4°C, the temperature was raised to 74°C with a 2°C/min gradient, and then decreased with the same rate. The CD signal intensity was recorded at 220 nm every 0.2°C. To determine the fraction of native headpiece at each temperature, the native and denatured states were defined as follows: the 4°C conformation of the non-irradiated headpiece was considered as the native one and the 74°C conformation, as the denatured one. Figure 2 shows the denaturation curves of a non-irradiated and a 700 Gy irradiated sample. Whereas the denaturation of the non-irradiated headpiece was completely reversible, this was not the case for the irradiated protein. Indeed, only 50 % of the fraction of a 700 Gy irradiated headpiece sample was structured before denaturation and this value falls to 30% after the denaturation - renaturation cycle. Moreover the thermal stability of the sample is lowered since the  $T_m$  decreases upon irradiation from 43.5°C to 40°C.

### *Fluorescence study of the state of the tyrosine residues*

The destruction of the tyrosine side-chains (tyrosines 7, 12, 17 and 47) upon irradiation was followed by the decrease of intrinsic fluorescence of the peptide. In the absence of other aromatic residues, intrinsic fluorescence is exclusively due to tyrosines. The headpiece was irradiated in solution within the dose range 0-2000 Gy ( $\lambda_{\text{excitation}} = 275$  nm, and emission spectra recorded from 280 to 350 nm). As shown in Figure 3A, the fluorescence of the headpiece decreases with increasing dose, without any change in the shape of the spectra. This decrease shows that tyrosine residues are degraded. Moreover, the evolution of the intrinsic fluorescence cannot be fitted with a simple exponential curve, which suggests that one or several tyrosine residues may be degraded faster than others.

Formation of dityrosines was observed by fluorescence measurements of the same samples using  $\lambda_{\text{excitation}} = 320$  nm. Emission spectra were recorded from 360 to 490 nm). Figure 3B shows the increase of fluorescence intensity in the dityrosine emission band.

***Calculated relative probabilities of the headpiece residues reaction with OH radicals***

The RADACK model was used to determine the probability, for each residue, to react with hydroxyl radicals during irradiation. The location of the most reactive amino acids (Tyr, Met, His, Arg) in the three-dimensional structure (1LQC from PDB) is shown in Figure 4A, whereas in Figure 4B, Smoluchowski's spheres are attributed to the reactive hydrogen atoms of the amino acids (RADACK representation). The largest spheres correspond to Tyr residues. According to RADACK calculations some residues have a higher probability than others to be damaged during radiolysis (Figure 4C). The difference of values for the four Tyr residues reflects the influence of structure which modulates solvent accessibility and thus, probability of reaction with OH radicals. The reactions of OH radicals with the protein have an 88% relative probability to occur on the side chains and only 12% on the peptide backbone, because of the low accessibility of the reactive sites on the backbone in the compact structure of the headpiece.

***Study of the irradiated headpiece by mass spectrometry***

Mass spectrometry (MALDI-TOF MS and ESI-IT MS) and tandem mass spectrometry (ESI-IT MS/MS) experiments were performed to follow side chain damage on the headpiece.

The headpiece was first irradiated within the dose range 0-1000 Gy and analysed by MALDI-TOF MS. The headpiece was analysed along with calibrants for accurate mass determination as shown in Figure 5A. The headpiece mass as determined from the doubly charged protein ion is 6696.9 Da (theoretical average mass 6697.6 Da, error 0.7 Da). Figure 5B shows that protein irradiation leads to the appearance of new protein species with a mass difference of 16 or 14 Da. In linear mode, the resolution was insufficient to differentiate clearly between these two types of modifications. Moreover, sodium and potassium adducts can partially obscure multiple oxidations. However, oxidation events clearly follow a dose-dependant relationship: at 200 Gy, protein species with up to three events are observed, whereas at least five oxidation events are visible at 500 Gy. Each additional modification decreases the intensity of individual peaks by widening the distribution of oxidised species. Thus at 1000 Gy, peaks are no longer resolved. The mass spectra do not show evidence of peptide backbone breakage.

Analysis of the whole headpiece doesn't allow for the identification of individual oxidised residues. In order to better localise the oxidation sites, the irradiated headpiece samples were proteolysed. We used either endoproteinase ArgC, which cleaves on the carboxylic side of Arg, or endoproteinase GluC, which cleaves on the carboxylic side of Glu and in some conditions, Asp residues. The cleavage products were analysed by MALDI-TOF MS (Figure 6). No uncleaved headpiece is detectable with either enzyme at 150 minutes proteolysis (mass range not shown). However, some sites are only partially cleaved, such as Arg35 in the Val23-Arg51 peptide (Figure 6, bottom panel). Cleavage at Asp8 residue with endoproteinase GluC is not observed. The C-terminal peptide (theoretical mass 1029.2 Da) is not detected after ArgC cleavage. Three oxidations are observed in the Val23-Arg51 peptide, while no oxidation appears in Val23-Arg35. In fact, with the exception of the aforementioned peptide, all detected peptides bear one or more oxidations as evidenced by the presence of protein species with mass differences in multiples of 16 Da. Thus, sites of oxidation seem dispersed throughout the sequence.

To localise damages on the sequence more precisely, MS/MS in an ion trap was performed. Peptide fragmentation along the peptide backbone may allow for the identification and localisation of amino acid side-chain modifications. A headpiece sample was irradiated at a dose of 500 Gy and cleaved with endoproteinase ArgC. The sample was then desalted and analysed by ESI-IT MS. Several ions corresponding to mono-oxidised peptides were selected for fragmentation. The mono-oxidised peptides corresponding to sequences Met1-Arg22 and Val23-Arg51 produced useful fragmentation information with respect to oxidation (Figure 7A and 7B). Ions are annotated following the Roepstorff–Fohlmann–Biemann nomenclature [24].

Fragmentation mainly occurs at the amide bond and leads to  $b_n$  (charge carried by the N-terminal end) and  $y_n$  (charge carried by the C-terminal end) ions. In the case of the Met1-Arg22 peptide, both oxidised and non-oxidised  $b_{12}$  ions are observed. This shows that the oxidation can be borne by a residue located in the Met1-Tyr12 or in the Ala13-Arg22 region, respectively. From this ion pair and other pairs of oxidised/non-oxidised fragment ions we can deduce that the observed mono-oxidised ion corresponds to a mixture of peptides. Moreover, for the Met1-Arg22 peptide a series of internal fragments starting at Pro3 and at Thr5 are also observed (Table 1). The internal fragment series is informative as it shows with certainty that there is one oxidation in the Tyr12-Ser16 region. The oxidised  $b$  series (Figure 7A) shows at least one oxidation in the Met1-Glu11 region. The oxidised  $y$  series shows an oxidation in the Ala13-Arg22 region. Interestingly, the oxidised to non-oxidised  $y$  ion intensity ratio decreases strongly after Tyr12, while the oxidised to non-oxidised  $b$  ion intensity ratio increases beyond

Glu11. These observations reinforce the notion that, while different mono-oxidised species are present, a peptide oxidised at Tyr12 might significantly contribute to the overall ion intensity.

In addition to +16 Da fragments, a number of low intensity +14 Da b ions ( $b_{11}$  to  $b_{21}$ ) and a +14 Da  $y_{11}$  ion were observed. For the sake of clarity, these were not annotated on spectra or sequences. For fragments of the Val23-Arg51 peptide, the oxidised y series localises one oxidation in the Leu45-Arg51 region. The oxidised  $b_{38}$  and  $b_{42}$ - $b_{48}$  ions indicate possible oxidation in the Val23-Glu44 region, while only non-oxidised b ions appear in the Val23-Glu36 region. Together, these results suggest one probable oxidation in the Glu36-Glu44 region. Moreover, the oxidised to non-oxidised b ion intensity ratio increases beyond Glu44, which confirms the presence of at least one other, major oxidation site in the Leu45-Arg51 region.

## Discussion

Gene expression is a very finely regulated process. In the case of lactose operon, binding of the repressor to the operator blocks the expression of three enzymes involved in lactose metabolism ( $\beta$ -galactosidase, lactose permease, and thiogalactoside transacetylase). Only 10 copies of the repressor protein are present per wild type bacterial cell [25]. Consequently, any alteration to the repressor that triggers a loss of binding ability can have direct consequences on the expression of operon proteins. Having investigated the damage to operon DNA (15, 16) and the effect of radiation on the function of the repressor [12], we focus here on the damage to the protein.

The damage of the repressor headpiece, the repressor binding domain is the most likely cause of the radiation-induced loss of repressor-operator recognition. We have examined here its degradation by a combination of techniques : circular dichroism, fluorescence spectroscopy, mass spectrometry and Monte-Carlo simulation.

Figure 1 shows that the irradiation of the headpiece causes the decrease of the CD intensity and a shift of the maximum negative intensity to shorter wavelengths. This proves a partial loss of the helical structure of the protein as a result of irradiation. This effect on the structure of the DNA binding domain of the repressor can contribute to the loss of its ability to bind DNA.

It was previously shown that the denaturation of the repressor headpiece by heat or by addition of rising concentration of urea is reversible [26-28]. We have studied the thermal

denaturation of the irradiated headpiece. As shown on Figure 2, the thermal denaturation of the control non-irradiated headpiece up to 74°C is completely reversible. For the 700 Gy irradiated headpiece, the fraction of structured headpiece at 4°C is lower than that of the non-irradiated headpiece (only 50 % of the headpiece has a native-like structure). Moreover, after a denaturation - renaturation cycle, the protein doesn't recover its original conformation since only 30% of the headpiece is in a native state after cooling. Consequently, the thermal cycle results in an additional loss of structure of the irradiated headpiece. One explanation can be the following : every radiation-induced lesion does not lead to unfolding at 4°C and therefore some regions remain in a native-like metastable state. The heating of the headpiece brings these regions over an energy barrier and induces their unfolding. During cooling of the completely denatured headpiece, the energy barrier prevents these regions from recovering their initial structure.

The observed decrease of  $T_m$  upon irradiation is also consistent with the radiation-induced lesions leading to a partially unfolded protein.

According to RADACK calculations, all four tyrosine residues (Tyr7, Tyr12, Tyr17 and Tyr47) of the headpiece present a high probability of reaction with OH radicals and consequently are prone to damage upon irradiation. We could easily follow their degradation by fluorescence emission spectroscopy since the headpiece doesn't bear any tryptophan and phenylalanine residues and thus the intrinsic fluorescence of the protein is exclusively due to the tyrosine fluorescence. As shown in Figure 3, tyrosine residues are indeed destroyed upon irradiation. Degradation of tyrosine can lead to the formation of dityrosine and DOPA, each of them emitting fluorescence [29-31]. The possible formation of DOPA could not be followed because its spectrum would be hidden by that of native tyrosine, but dityrosine formation was observed. The inset of Figure 3A shows that the decrease of tyrosine fluorescence intensity doesn't fit a simple exponential curve. This means that the degradation rates of the four tyrosine residues are not the same and thus one or several residues might be damaged before the other ones. The production of dityrosine follows a sigmoidal curve (Fig. 3B). By molecular modeling, we have previously shown that the formation of dityrosine between Tyr7 and Tyr 17 (the closest to each other in the three-dimensional structure of the headpiece and belonging to the two helices of the HTH recognition motif) energetically disfavors the operator-headpiece complex [32]. However, the presence of the dityrosine adducts revealed by the fluorescence measurements was not observed in MALDI-TOF experiments. This could be explained by the presence of only a small proportion of dityrosine and of a high proportion of dityrosine-like fluorescence, such as the relatively abundant (but

chemically unidentified) species reported for irradiated RNase and lysozyme (accounting for 84% and 98% of the fluorescence, respectively) [31].

RADACK calculation shows that not only tyrosine, but also some other amino acids have a high probability to react with hydroxyl radicals. Mass spectrometry was used to search for direct evidence of modification on all residues of the headpiece.

While MALDI-TOF analysis of intact versus oxidised protein is only semi-quantitative in our conditions, we can infer that at least 10-15 % of the protein bears one or more oxidations at 100 Gy (Figures 5 and 6). According to our previous results and calculations in single hit statistics conditions [15, 33], 100 Gy are necessary to induce one or more strand breaks in 4 % of a DNA fragment of the size of the operator sequence (20 base pairs). Since the global number of damages (strand breaks and base damage) is three-fold that of strand breaks, around 12 % of the binding sequence will be damaged when DNA is irradiated with 100 Gy. Both partners thus bear a similar number of damages. However the effect on binding seems different: at this dose damage to the repressor directly affects complex formation, whereas damage to operator DNA has no effect [12]. A quantitative comparison is nevertheless not straightforward. Not only will damage to the headpiece lead to the destruction of the complex, but damage to the other part of the repressor (known as the core) may also contribute. It is known that binding of isopropyl-1- $\beta$ -D-thiogalactoside to the core changes the headpiece spatial orientation and thus hinders repressor-operator binding. Through similar allosteric effects, radiation-induced lesions to the core can affect headpiece binding to DNA, leading to an even greater sensitivity of the whole repressor to oxidation compared with the headpiece alone.

The study of the whole irradiated headpiece by MALDI-TOF shows that several side chains are oxidised upon irradiation. Proteolysis of the irradiated headpiece reveals the oxidised regions of the protein, while MS/MS analysis narrows them down.

By confronting the experimental mass spectrometry results with RADACK prediction we can pinpoint the most likely hotspots of radiation-induced damage of the headpiece. The oxidation observed in the Met1-Glu11 region may correspond either to damage to Met 1 or to Tyr7. According to RADACK, the probability of damage of Tyr 7 is much higher than that of Met1. The oxidation in the Tyr12-Ser16 region point towards damage of Tyr12. The oxidation in Ala13-Arg22 region may correspond to the oxidation of Tyr17. The oxidation of Val23-Glu44, without any oxidation in Val23-Glu36 is consistent with an oxidation of Met42. In the Leu45-Arg51 region, although Arg51 may contribute, according to RADACK the strongest oxidation is likely to be localised at Tyr47. In the Val23-Arg51 peptide, two of the

three observed oxidations can thus be due to oxidation of Met42 and Tyr47. The third oxidised residue can be His29, Arg35 or Arg51. No positive evidence is available to unambiguously decide between these three possibilities. Table 2 summarises the conclusions of the discussion of mass spectrometry data in light of RADACK predictions.

The identification of tyrosines as the most probable hotspots of oxidation is consistent with the loss of intact tyrosines observed by fluorescence. Moreover, given the location of Tyr7, Tyr 12 and Tyr17 in the two helices of the HTH motif, one can easily understand the radiation-induced loss of helical structure observed by circular dichroism. The loss of binding ability of the repressor to operator DNA upon irradiation is thus probably based on the loss of recognition function of the headpiece HTH motif.

Until now, radiation-induced damage of proteins has been successfully used as a tool for probing protein structure and interactions in cases where three-dimensional structure of the protein or of protein complexes is not available [34-36]. Here we have shown that a combination of analytical methods can be used to determine the radiation-induced damage of a DNA-binding protein with a known structure.

Our results reveal alterations of a protein upon irradiation and show that its loss of function is correlated with conformational changes and chemical modifications. The damage to the protein is one of the initial radiation-induced events, which under the influence of the cellular environment and after processing by cellular mechanisms, are involved in the deleterious effects of ionising radiation *in vivo*.

In the cell a DNA-binding protein is not only in the presence of its partner DNA sequence, but also in the presence of many other molecules. These can act as radioprotectors by scavenging OH radicals, by shielding the target residues, and by chemical repair. They can, however, also act as radiosensitisers. All molecules, even radioprotectors, are attacked by the OH radicals, and reactive radicals are formed on them. These secondary radicals will inflict additional damage on the protein [37]. Thus, for a dose where an isolated protein in solution is only slightly damaged, *in vivo* the same protein could sustain much more damage if the radiosensitisation overcomes the protection. The overall effect is a sum of all radioprotective and radiosensitising effects. In addition, protein oxidation leads to reduced proteasome-mediated degradation, accumulation of unfolded protein and a number of other phenomena which contribute to amplify the effect of the initial damage at the cellular level.

Interestingly, in spite of the complexity of the cellular environment, doses inducing measurable damage to the repressor headpiece in our *in vitro* study are in the same range as those affecting whole *E. coli* cells survival. For instance, a dose of 100 Gy that induces the

oxidation of about 10% of the headpiece reduces the survival of wild-type *E. coli* by 10-20 % [38]. While we cannot conclude on a direct relationship between the damage to the repressor molecule and the reduced survival of *E. coli* due to the complexity of the *in vivo* system, the idea that dysfunction of the lactose operon possibly contributes to the fitness or viability of the bacteria is intriguing.

## Conclusion

Upon irradiation the lactose repressor loses its ability to bind the operator DNA. This is most probably due to damage to its DNA binding domain, the headpiece. We have shown here that this domain undergoes a radiation-induced conformational change due to the damage (mainly oxidation) of amino acids. At 4°C, some regions lose their helical structure, whereas others are in a metastable state. The oxidation occurs gradually with increasing dose, starting with the amino acids presenting the highest accessibility and the highest reactivity toward OH radicals. By confronting the experimental results with RADACK prediction we conclude that Tyr 7, Tyr12, Tyr17, Met42 and Tyr47 are the most likely hot spots of oxidation. Our results shed light on the modifications of a protein upon irradiation and show that chemical modifications and conformational changes are correlated with the radiation-induced loss of its function. This result is relevant for the understanding of cellular effects of ionising radiation because protein damage is one of the multiple radiation-induced primary events, that under the influence of the cellular environment and after processing by cellular mechanisms, are involved in the deleterious effects of ionising radiation *in vivo*.

## Acknowledgements

This work was supported by a grant from *Electricité de France*, by a grant from *Association pour la Recherche contre le Cancer* (ARC), by the European COST action “Radiation damage in biomolecular systems” and by the bilateral Czech-French program of scientific collaboration Barrande. M.C. is grateful to the CNRS for the award of an ATIP grant.



## REFERENCES

1. Cadet J., Douki T., Gasparutto D. and Ravanat J.-L. (2003) Oxidative damage to DNA: formation, measurement and biochemical features. *Mutat. Res.* **531**, 5-23
2. Fu, S., Davies, M.J., Stocker, R. and Dean, R.T. (1998) Evidence for roles of radicals in protein oxidation in advanced human atherosclerotic plaque. *Biochem. J.* **333**, 519-525.
3. Brillard-Bourdet, M., Hamdaoui, A., Hajjar, E., Boudier, C., Reuter, N., Ehret-Sabatier, L. Bieth, J.G. and Gauthier, F. (2006) A novel locust (*Schistocerca gregaria*) serine protease inhibitor with a high affinity for neutrophil elastase. *Biochem. J.* **400**, 467-476.
4. Garrison, W.M. (1987) Reaction mechanisms in the radiolysis of peptides, polypeptides, and proteins. *Chem. Rev.* **87**, 381-398
5. Stadtman, E.R. (1993) Oxidation of free amino acids and amino acid residues in protein by radiolysis and by metal-catalysed reactions. *Annu. Rev. Biochem.* **62**, 797-821
6. Buxton, G.V., Greenstock, C. L., Helman, W. P. and Ross, A.B. (1988) Critical review of rate constants for reactions of hydrated electrons, hydrogen atoms and hydroxyl radicals ( $\text{OH}\cdot$ ,  $\text{O}^{\cdot-}$ ) in aqueous solution. *J. Phys. Chem. Ref. Data* **17**, 513-886
7. Finley, E. L., Dillon, J., Crouch; R.K. and Schey, K.L. (1998) Radiolysis-induced oxidation of bovine  $\gamma$ -crystalline. *Photochem. Photobiol.* **68**, 9-15
8. Audette, M., Blouquit, Y. and Houée-Lévin, C. (2000) Oxidative dimerization of protein: role of tyrosine accessibility. *Arch. Biochem. Biophys.* **376**, 217-220
9. Begusova, M. Spothem-Maurizot, M. Sy, D., Michalik, V. and Charlier, M. (2001) RADACK, a stochastic simulation of hydroxyl radical attack to DNA. *J. Biomol. Struct. Dyn.* **19**, 141-158

10. Gillard, N., Begusova, M., Castaing, B. and Spothem-Maurizot, M. (2004) Radiation affects binding of Fpg repair protein to an abasic site containing DNA. *Radiat. Res.* **162**, 566-571
11. Begusova, M., Gillard, N., Sy, D., Castaing, B., Charlier, M. and Spothem-Maurizot, M. (2005) Radiolysis of DNA-protein complexes. *Radiat. Phys. Chem.* **72**, 265-270
12. Eon, S., Culard, F., Sy, D., Charlier, M. and Spothem-Maurizot, M. (2001) Radiation disrupts protein-DNA complexes through damage to the protein. The *lac* repressor-operator system. *Radiat. Res.* **156**, 110-117
13. Charlier, M., Eon, S., Sèche, E., Bouffard, S., Culard, F. and Spothem-Maurizot, M. (2002) Radiolysis of *lac* repressor by  $\gamma$  rays and heavy ions. A two hits model for protein inactivation. *Biophys. J.* **82**, 2373-2382
14. Culard, F., Gervais, A., de Vuyst, G., Spothem-Maurizot, M. and Charlier, M. (2003) Response of a DNA-binding protein to radiation-induced oxidative stress. *J. Mol. Biol.* **328**, 1185-1195
15. Franchet-Beuzit, J., Spothem-Maurizot, M., Sabattier, R., Blazy-Baudras, B. and Charlier, M. (1993) Radiolytic footprinting.  $\beta$  rays,  $\gamma$  photons and fast neutrons probe DNA-protein interactions. *Biochemistry* **32**, 2104-2110
16. Begusova, M., Eon, S., Culard, F., Charlier, M. and Spothem-Maurizot, M. (2001) Radiosensitivity of DNA in a specific protein-DNA complex: the *lac* repressor-*lac* operator complex. *Int. J. Radiat. Biol.* **77**, 645-654
17. Kalodimos, C.G., Folkers, G.E., Boelens, R. and Kaptein, R. (2001) Strong DNA binding by covalently linked dimeric *Lac* headpiece: evidence for the crucial role of the hinge helices. *Proc. Natl. Acad. Sci. USA* **98**, 6039-44
18. Kalodimos, C.g., Bonvin, A.M., Salinas, R.K., Wechselberger, R., Boelens, R. and Kaptein, R. (2002) Plasticity in protein-DNA recognition: *lac* repressor interacts with its

natural operator O1 through alternative conformations of its DNA-binding domain. *Embo J.* **21**, 2866-76

19. Kalodimos, C.G., Boelens, R. and Kaptein, R. (2002) A residue-specific view of the association and dissociation pathway in protein-DNA recognition. *Nat. Struct. Biol.* **9**, 193-197

20. Spronk, C.A., Slijper, M., van Boom, J.H., Kaptein, R. and Boelens, R. (1996) Formation of the hinge helix in the *lac* repressor is induced upon binding to the *lac* operator. *Nat. Struct. Biol.* **3**, 916-9

21. Chuprina, V.P., Rullmann, J.A., Lamerichs, R.M., van Boom, J.H., Boelens, R. and Kaptein, R. (1993) Structure of the complex of *lac* repressor headpiece and an 11 base-pair half-operator determined by nuclear magnetic resonance spectroscopy and restrained molecular dynamics. *J. Mol. Biol.* **234**, 446-62

22. Slijper, M., Bonvin, A.M., Boelens, R. and Kaptein, R. (1996) Refined structure of *lac* repressor headpiece (1-56) determined by relaxation matrix calculations from 2D and 3D NOE data: change of tertiary structure upon binding to the *lac* operator. *J. Mol. Biol.* **259**, 761-73

23. Cadène, M. and Chait, B.T. (2000) A robust, detergent-friendly method for mass spectrometric analysis of integral membrane proteins. *Anal. Chem.* **72**, 5655-5658

24. Biemann, K. (1992) Mass spectrometry of peptides and proteins. *Annu. Rev. Biochem.* **61**, 977-1010.

25. Gilbert, W. and Müller-Hill, B. (1966) Isolation of the Lac repressor *Proc. Natl. Acad. Sci. USA* **56**, 1891-1898.

26. Schnarr, M. and Maurizot, J.C. (1982) Secondary structure of the *lac* repressor headpiece. Possibilities and limitations of a joint infrared and circular dichroism study. *Eur J Biochem.* **128**, 515-520

27. Schnarr, M. and Maurizot, J.C. (1982) Stability of the lac repressor headpiece against thermal denaturation and tryptic hydrolysis. *Biochim Biophys Acta* **702**, 155-162
28. Schnarr, M. and Maurizot, J.C. (1981) Unfolding of lac repressor and its proteolytic fragment by urea: headpieces stabilize the core within lac repressor. *Biochemistry* **20**, 6164-9
29. Jain R., Freund, H.G., Budzinsky, E. and Sharma, M. (1997) Radiation-induced formation of 3,4-dihydroxyphenylalanine in tyrosine-containing peptides and proteins as a function of X-irradiation dose. *Bioconjugate Chemistry*. **8**, 173-178
30. Karam, L.R., Dizdaroglu, M. and Simic M.G. (1984) OH radical induced products of tyrosine peptides. *Int. J. Radiat. Biol.* **46**, 715-724
31. Huggins, T.G., Wells-Knecht, M.C., Detorie, N.A., Baynes, J.W. and Thorpe, S. (1993) Formation of *o*-tyrosine and dityrosine in proteins during radiolytic and metal-catalysed oxidation. *J. Biol. Chem.* **268**, 12341-12347
32. Gras, J., Sy, D., Eon, S., Charlier, M. and Spothem- Maurizot, M. (2005) Consequences of intramolecular dityrosine formation on a DNA-protein complex. A molecular modeling study. *Radiat. Phys. Chem.* **72**, 271-278
33. Spothem-Maurizot, M., Charlier, M. and Sabattier, R. (1990) DNA radiolysis by fast neutrons. *Int. J. Radiat. Biol.* **57**, 301-313
34. Xu, G., Chance, M.R. (2005) Radiolytic Modification and Reactivity of Amino Acid Residues Serving as Structural Probes for Protein Footprinting. *Anal. Chem.* **77**, 4549-55.
35. Guan, J.Q., Chance, M.R. (2005) Structural proteomics of macromolecular assemblies using oxidative footprinting and mass spectrometry. *Trends Biochem Sci* **30**, 583-92.
36. Takamoto, K.G., Chance, M.R. (2006) "Radiolytic protein footprinting with mass spectrometry to probe the structure of macromolecular complexes", *Annual Review of Biophysics and Biomolecular Structure*, Volume 35, 251-276.

37. Nauser, T., Koppenol, W.H. and Gebicki, J.M. (2005) The kinetics of oxidation of GSH by protein radicals. *Biochem. J.* **392**, 693-701

38. Boubrik, F. and Rouviere-Yaniv, J. (1995) Increased sensitivity to  $\gamma$  irradiation in bacteria lacking protein HU. *Proc. Natl. Acad. Sci. USA* **92**, 3958-3962

## Figures titles and legends

### Figure 1.

#### **Secondary structure of the irradiated headpiece.**

CD spectra of the headpiece irradiated in the dose range 0-2000 Gy in a buffer containing 25 mM ammonium cacodylate, pH 7.25. The protein concentration was 29  $\mu$ M. The inset shows the normalised variation of ellipticity at 220 nm

### Figure 2.

#### **Thermal denaturation-renaturation cycle of intact and irradiated headpiece.**

Fraction of structured headpiece as a function of temperature during a denaturation-renaturation cycle, deduced from CD measurements. The cycle was performed for unirradiated (full line) and a 700 Gy irradiated (dashed lines) sample.  $f_T = (\epsilon_T - \epsilon_d) / (\epsilon_{nd} - \epsilon_d)$  where  $\epsilon_T$ ,  $\epsilon_d$ ,  $\epsilon_{nd}$  are the variations of ellipticity at 220 nm of the headpiece at the temperature T, in the structured and in the denatured states, respectively.

### Figure 3.

#### **Tyrosine and dityrosine band fluorescence of the irradiated headpiece.**

A. Fluorescence emission spectra of the headpiece as a function of dose (range: 0-2000 Gy;  $\lambda_{excitation} = 275$  nm). The inset shows, in the emission band of tyrosine, the decrease of the fluorescence intensity as a function of dose. B. Dityrosine band fluorescence emission spectra of the headpiece as a function of dose (range:0-2000 Gy;  $\lambda_{excitation} = 320$  nm). The inset shows, in the emission band of dityrosine, the increase of the fluorescence intensity versus the dose.

### Figure 4.

#### **RADACK prediction of the damaged sites.**

Probability of reaction of headpiece amino acids with OH radicals as calculated with the RADACK model using the NMR-based structure available in the PDB Databank with the code 1LQC [18]. A. Location of the most reactive amino acids in the headpiece. B. RADACK representation of the headpiece with Smoluchowski's spheres on the reactive atoms (the headpiece position and the colors used for the

amino acids are the same as in panel A). C. Calculated relative probabilities of reaction of each amino acid with OH radicals.

**Figure 5.**

**Oxidation of the whole headpiece.**

A. MALDI-TOF spectrum of the unirradiated headpiece analysed with a set of calibrants (c). B. MALDI-TOF spectrum of irradiated samples of headpiece (29  $\mu$ M in 25 mM ammonium cacodylate buffer, pH 7.25) in the dose range of 0 to 1000 Gy.

**Figure 6.**

**Oxidation of proteolytic peptides of the irradiated headpiece.**

Top panel: MALDI-TOF spectra of the unirradiated headpiece proteolysed by endoproteinase ArgC (A) or GluC (B). Middle panel: 80 Da spectrum windows on proteolytic peptides of irradiated headpiece (0 to 1000 Gy). Oxidised species are marked with an asterisk, triangles indicate Na<sup>+</sup> and/or K<sup>+</sup> adducts. The species marked ° is unidentified (1295.4Da). Bottom panel: Summary of oxidations observed by MALDI-TOF. The residues that were shown by RADACK calculation as having the greatest probabilities to react with hydroxyl radicals are shown in gray on the sequence. Potential target residues for proteolysis bear numbers. The theoretical average mass of singly charged intact peptides is indicated, as well as observed oxidations.

**Figure 7.**

**Localisation of oxidations in irradiated headpiece peptides.**

Ion-trap fragmentation of mono-oxidised ArgC cleavage peptides of the headpiece irradiated at 500 Gy. ESI-IT MS/MS spectra of (A) triply charged [M1-R22] peptide, precursor m/z 832.2Da (for the sake of clarity, the 4 most intense ions are left off-scale), and (B) quadruply charged [V23-R51] peptide, precursor m/z 811.7Da. Diamonds indicate the precursor ions.

Spectra annotations reflect b<sub>n</sub> and y<sub>n</sub> ions as well internal ions labelled "i". Oxidised species are topped with an asterisk (b<sub>n</sub><sup>\*</sup> and y<sub>n</sub><sup>\*</sup> ions) The sequence is annotated once for each fragmentation site irrespective of the number of observed

charge states for the fragment. For clarity, internal ions were not reported on the sequence and are listed in Table1.



## Tables

**Table 1 : Oxidation state of internal fragments of mono-oxidised Met1-Arg22 peptide observed in ESI-IT MS/MS.**

Fragment sequence	without oxidation	oxidised
3PVTLYDVAEYAGVS 16	yes	yes
3PVTLYDVAEYAGV 15	yes	
3PVTLYDVAEYAG 14	yes	
3PVTLYDVAEYA 13	yes	yes
3PVTLYDVAEY 12	yes	yes
3PVTLYDVAE 11	yes	
3PVTLYDV9	yes	
3PVTLYD8	yes	
PV5TLYDVAEYAGVS 16	yes	

**Table 2. Hotspots of radiolytic oxidation as deduced from a combination of mass spectrometry and RADACK data.**

Headpiece regions	Number of oxidations	Most probable hotspot
Met1-Glu11	1	Tyr7
Tyr12-Ser16	1	Tyr12
Ala13-Arg22	1	Tyr17
Lys37-Glu44	1	Met42
Leu45-Arg51	1	Tyr47

**Figure 1**

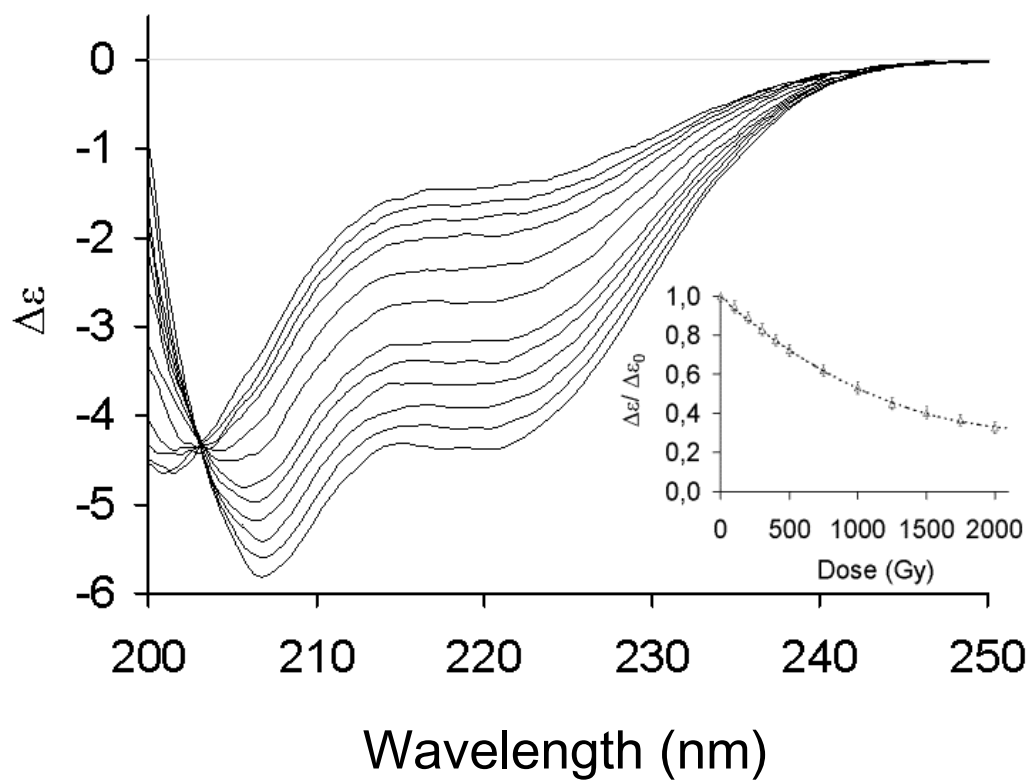


**Figure 2**

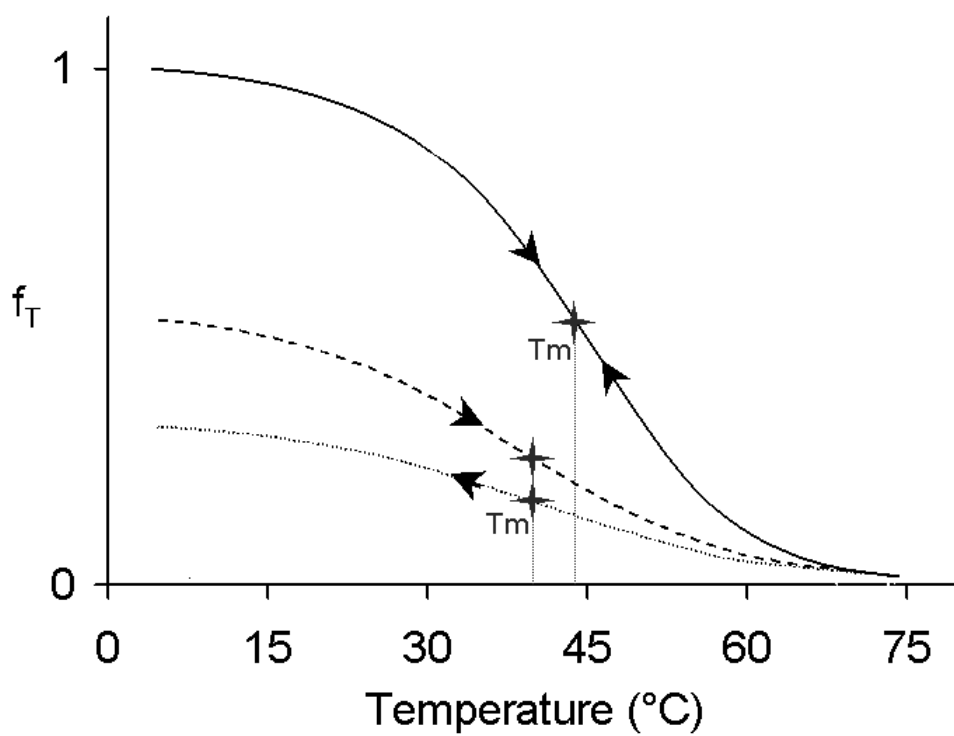


Figure 3

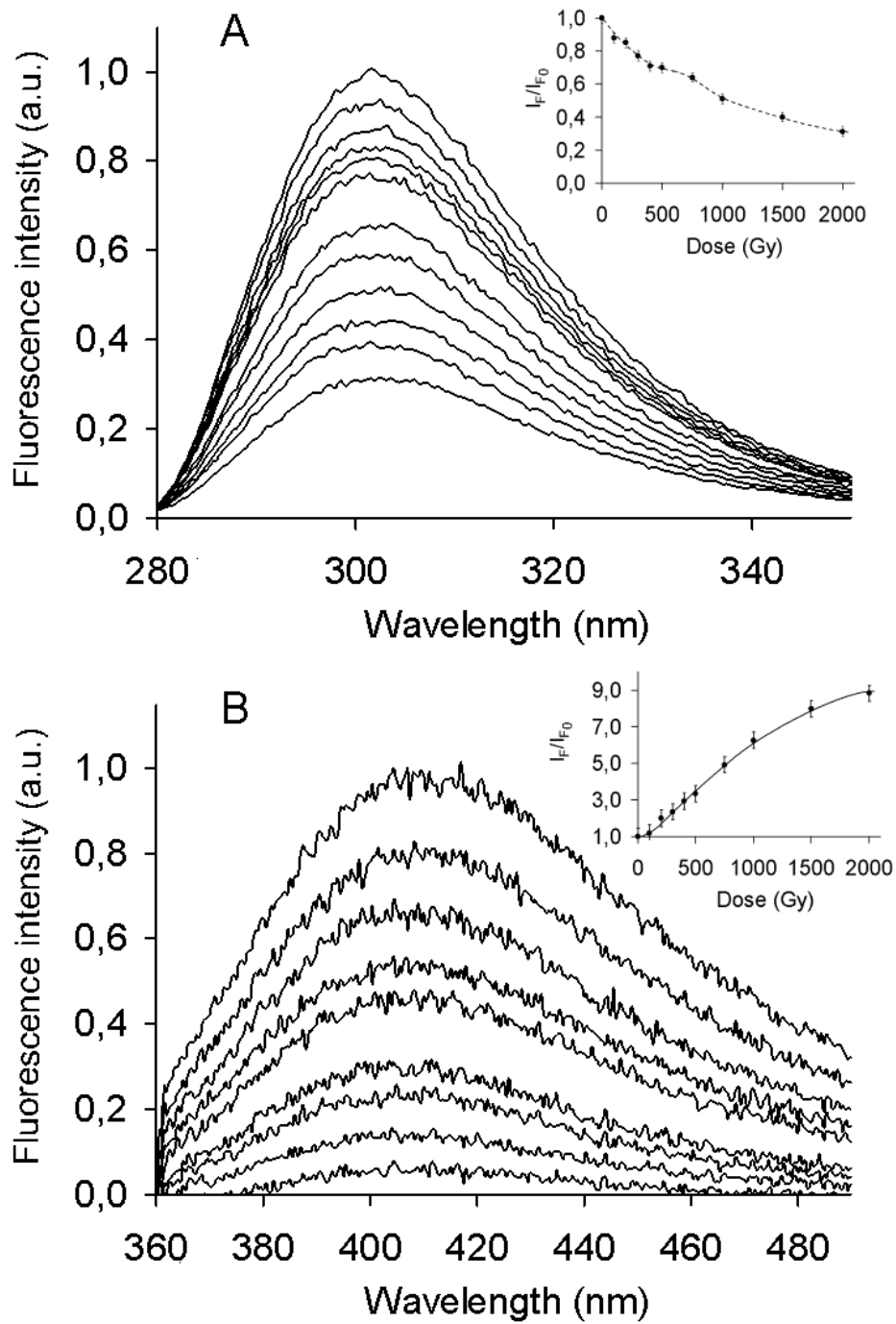
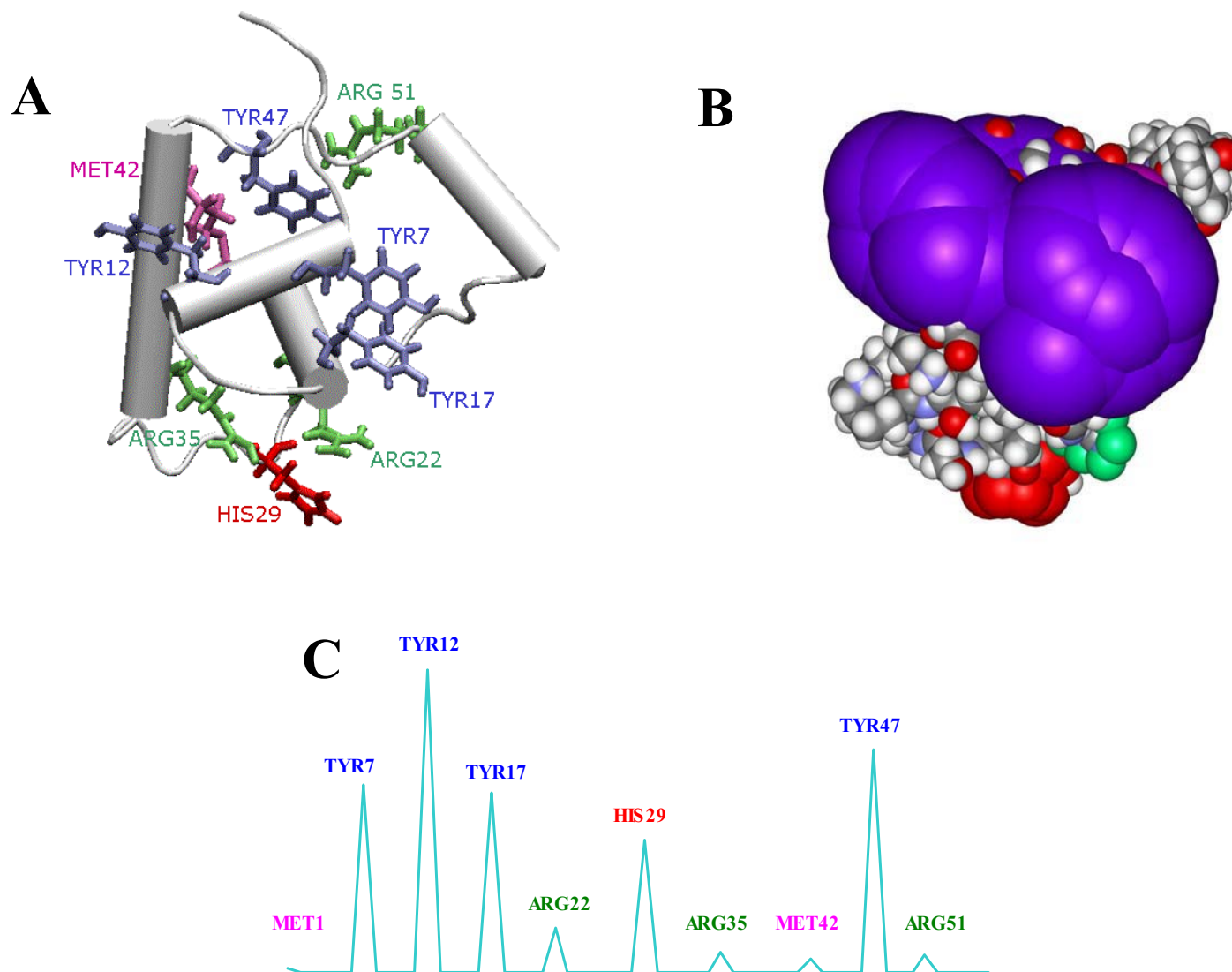
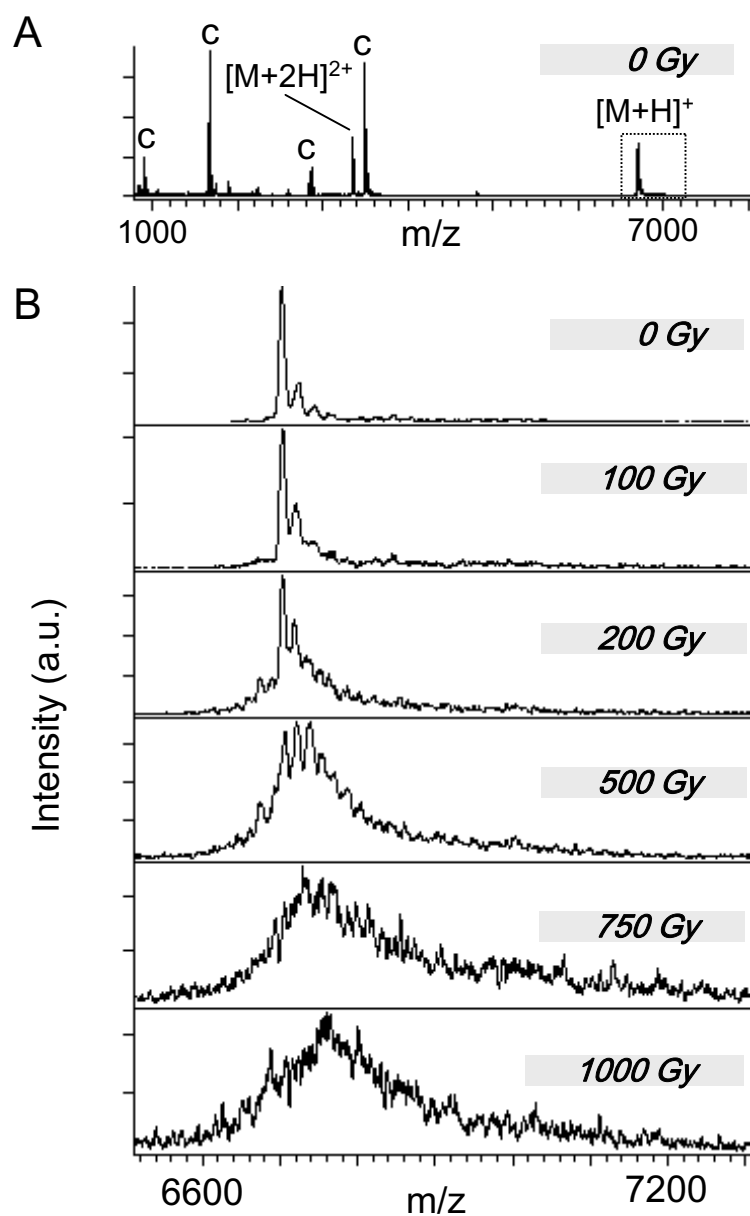


Figure 4



**Figure 5**



**Figure 6**

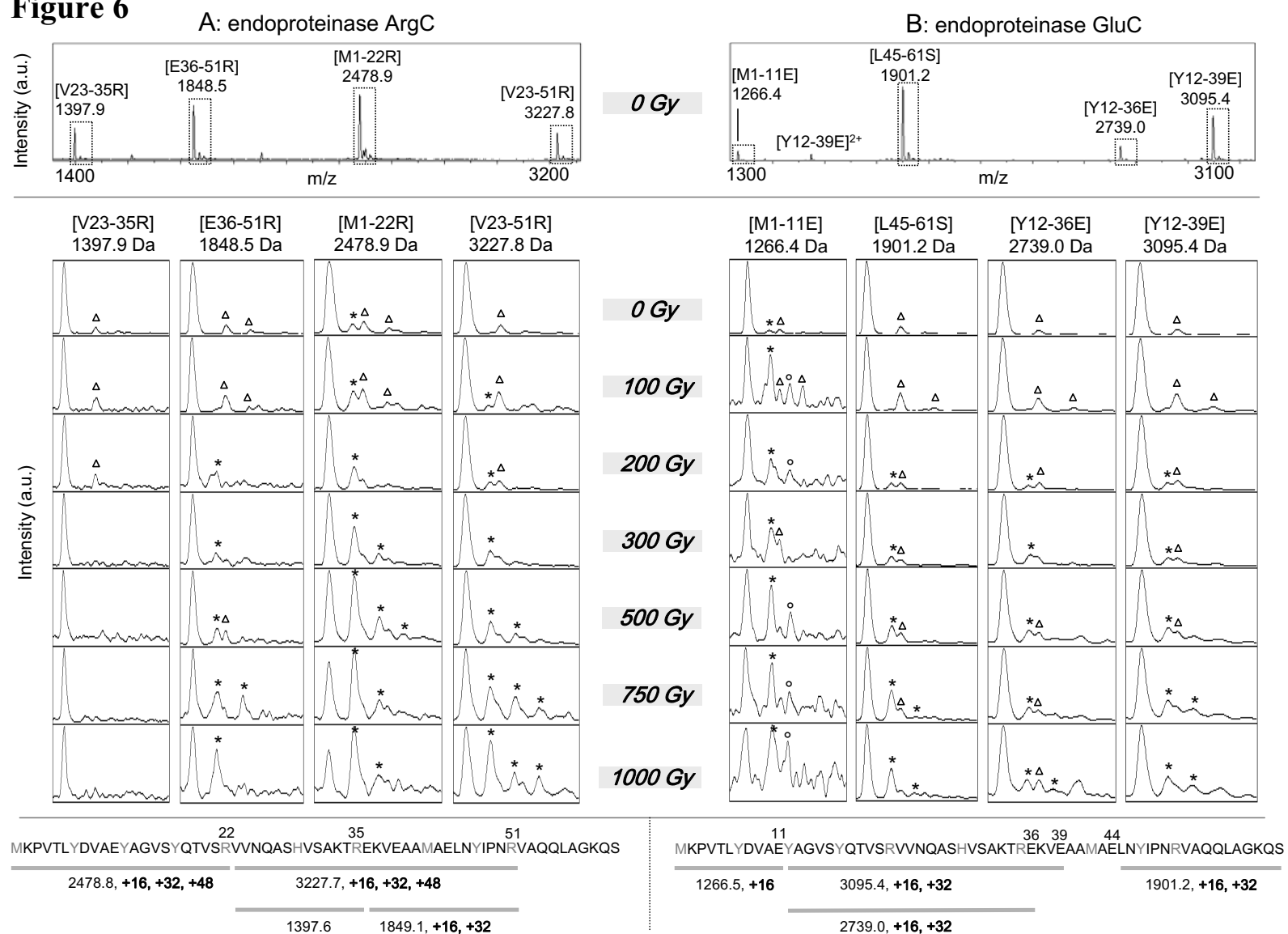


**Figure 7A**

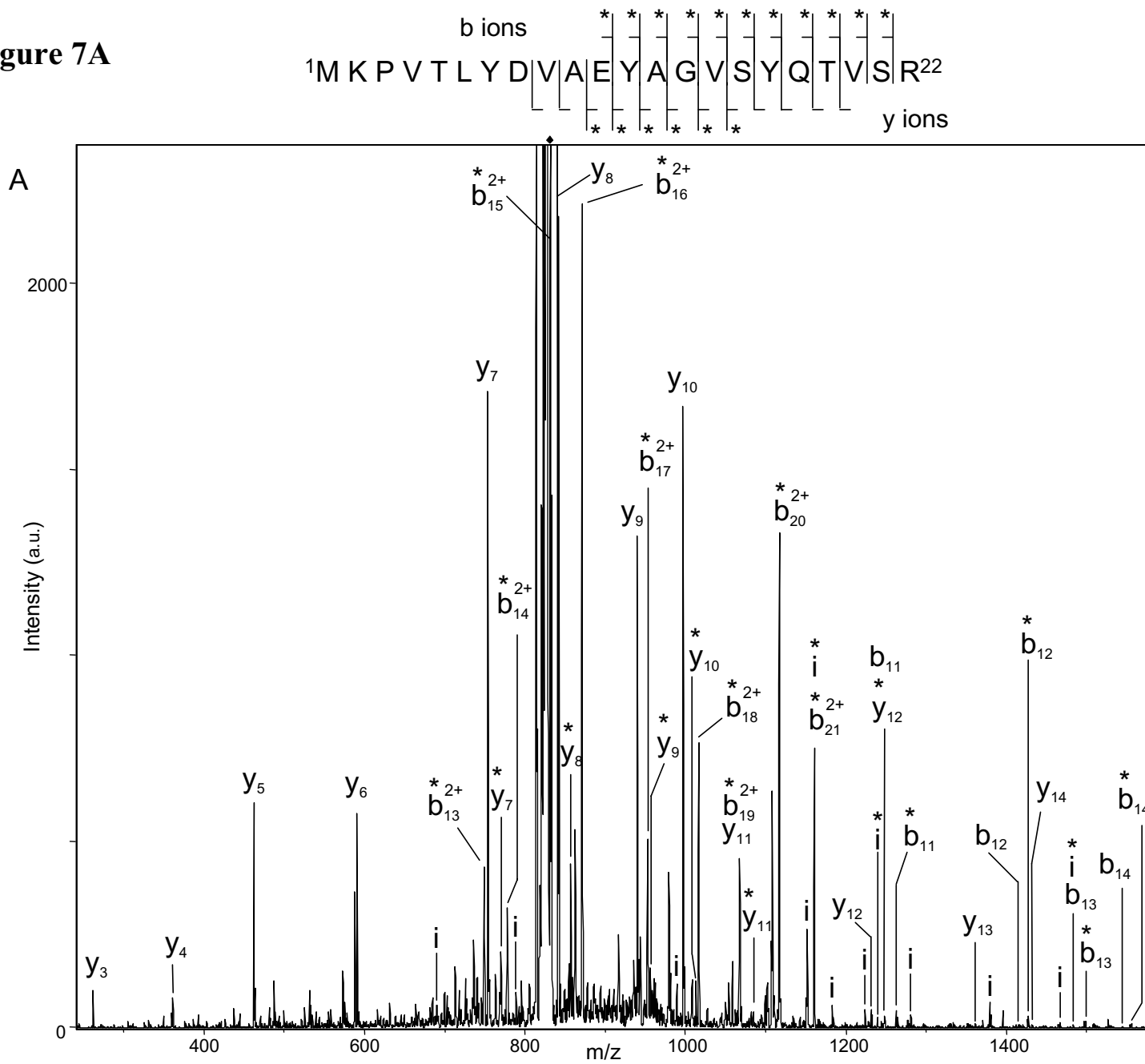




**Figure 7B**

